LATVIAN JOURNAL OF PHYSICS AND TECHNICAL SCIENCES
2012, N 5
DOI: 10.2478/v10047-012-0028-y

*BIOPHOTONICS*

# BIOPHOTONIC TECHNOLOGIES FOR NON-INVASIVE ASSESSMENT OF SKIN CONDITION AND BLOOD MICROCIRCULATION

J. Spigulis

Biophotonics Laboratory, Institute of Atomic Physics and Spectroscopy
University of Latvia,
19 Raina Blvd., Riga, LV-1586, LATVIA
e-mail: janis.spigulis@lu.lv

The main results obtained at the author's laboratory over the recent five years with respect to optical *in-vivo* skin assessment are reviewed. The exploited optical properties of human skin are briefly regarded, with following description of the newly developed methods and prototype devices. In particular, six non-invasive diagnostic and monitoring technologies based on skin autofluorescence photobleaching, diffuse reflectance spectrometry, multispectral skin imaging, and remission photoplethysmography have been proposed, experimentally implemented, and clinically tested.

**Key words**: *distant skin assessment, skin fluorescence, skin chromophore mapping, photoplethysmography.*

## 1. INTRODUCTION

Five key emerging technologies have recently been identified as Europe-2020 strategic priorities [1], including photonics – and biophotonics as its part. Biophotonics is an inter-disciplinary R&D area aiming at improved quality of life assisted by advanced optical technologies. As compared with the traditional clinical approaches, biophotonic techniques have several advantages – including the possibility of patient-friendly non-invasive and even non-contact diagnostics and monitoring of the health condition, e.g. evaluation of skin pathologies and blood microcirculation. This has been a research topic at the Biophotonics Laboratory of Institute of Atomic Physics and Spectroscopy (University of Latvia) over the recent years (studied in the frame of several national and European projects).

This paper presents the basic concepts on skin optics and summarises our main results obtained during the years 2007–2012. Description is given for the developed non-invasive diagnostic and monitoring technologies based on skin autofluorescence photobleaching, diffuse reflectance spectrometry, multispectral skin imaging and remission photoplethysmography.

## 2. OPTICAL PROPERTIES OF HUMAN SKIN: THE BASICS

Human skin has a complicated layered structure as illustrated in Fig. 1*a*. The two main layers (shown in Fig. 1*b*) below the external *Stratum Corneum* (~10–20 microns thin, consists of dead cells) are *Epidermis* (~100–150 microns thin

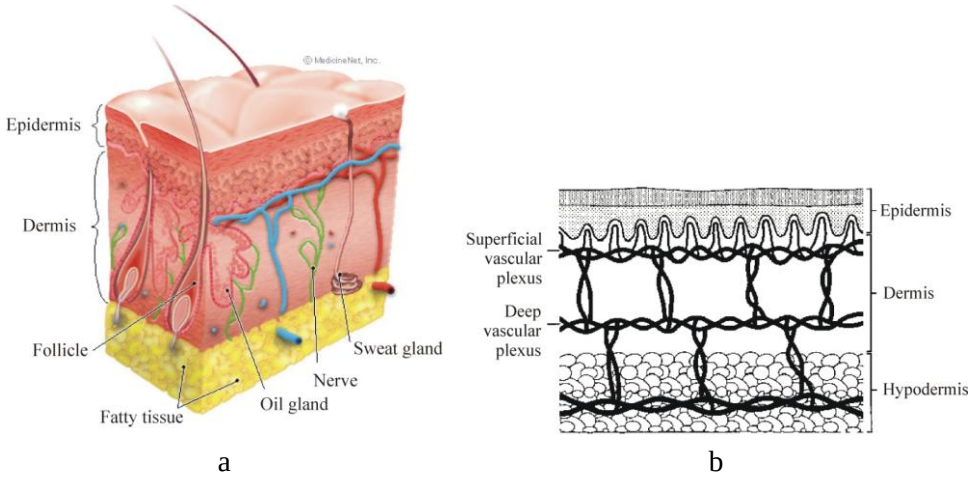


a b

*Fig. 1.* Layered structure of human skin (*a*) and cutaneous vascular system (*b*) [2].

jelly-like substance without blood vessels) and *Dermis* (up to 3–4 mm, comprising upper capillaries and deeper vascular structures) The incident light can be reflected from the skin surface and also may enter the epidermal and dermal layers where it can be absorbed and/or scattered (Fig. 2*a*). If the absorption probability is low, a portion of the scattered light is back-scattered or remitted and can be detected a few millimetres apart from the light source (Fig. 2*b*). In such conditions a fraction of the detected photons have been travelled via the dermal layer where the blood volume periodically changes with each heartbeat – arteries and arterioles are simultaneously expanding and contracting due to the changeable blood pressure. As a consequence, the detected so-called remission photoplethysmography (PPG) signal comprises a relatively stable DC component determined by absorption of the "static" skin structures, and a pulsatile AC component caused by the periodically changing blood absorption, so reflecting both the heart functioning and the vascular properties [4]. Light losses in skin are determined by the radiation wavelength and by concentration of the skin absorbers called chromophores; the most essential of them are: (i) melanin, located in the epidermal layer; (ii) oxy- and deoxy-haemoglobin – a constituent of blood erythrocytes located in the dermal layer; and (iii) water as a constituent of all living cells. Figure 3*a* compares their absorption spectra; a considerable scattering and remission can be expected only in the low

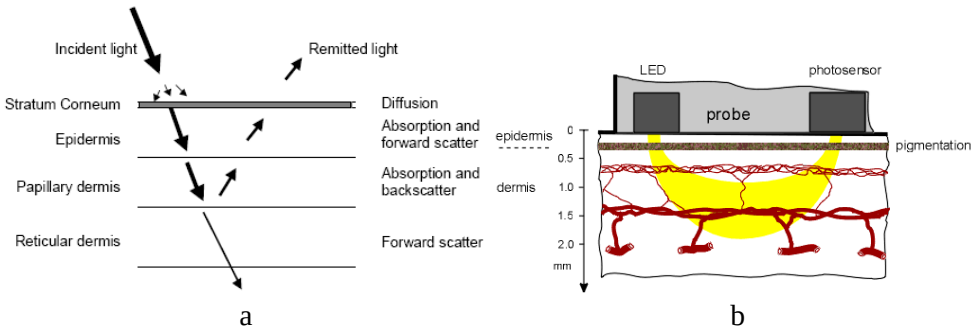


a b

*Fig. 2.* Light propagation in the skin layers (*a*) and detection of the remitted light by a photoplethysmography probe (*b*) [3].

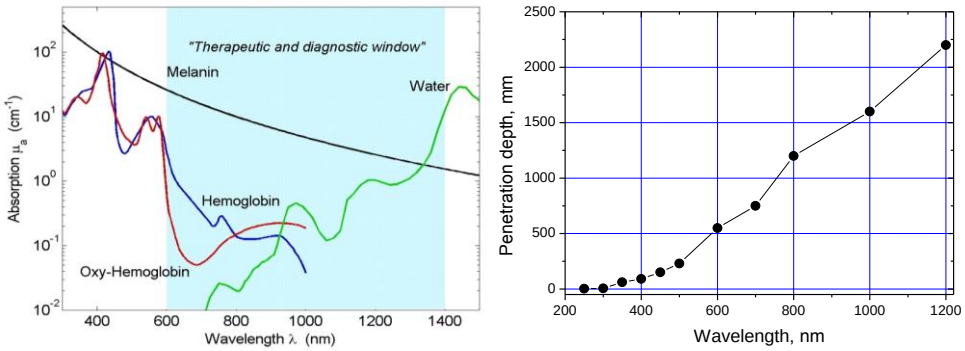


a b

*Fig. 3.* Absorption spectra of the main skin chromophores [5] (*a*) and spectral dependence of the mean penetration depth of light in skin [6] (*b*).

absorbance region (600–1300 nm) called "therapeutic window" – the mean penetration depth of light (where the incident intensity decreases by factor 1/e) in this region varies between 0.5…2 mm depending on the wavelength (Fig. 3*b*). If the light is absorbed in skin, it can be further re-emitted at longer wavelengths as the autofluorescence, i.e. self-fluorescence without any specific additives on or inside the skin. There is a number of fluorescing compounds called fluorophores in the upper skin, each with its specific emission spectrum (Fig. 4).

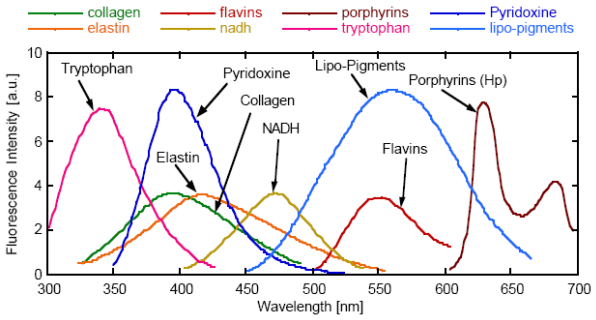


*Fig. 4*. Emission spectra of endogenous skin fluorophores [7].

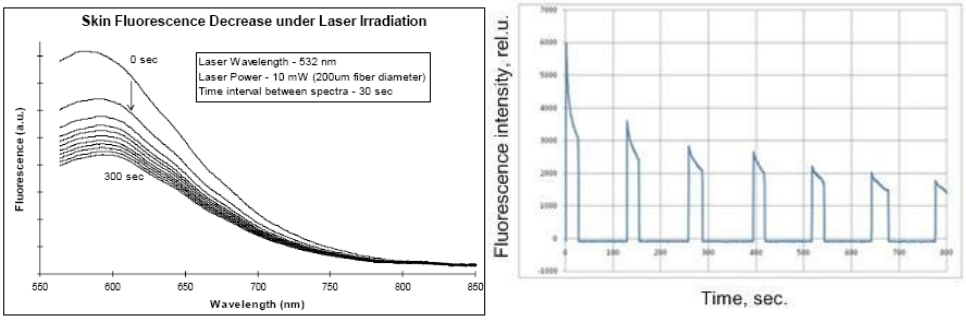


a b

*Fig.5*. Skin autofluorescence photobleaching at continuous 532 nm laser irradiation (10–85 mW/cm$^2$): *a* – temporal changes of the emission spectrum [8], *b* – partial recovery of the autofluorescence intensity after interrupted excitation [9].

Even if excited by a narrow laser line, several emission spectra overlap and the skin autofluorescence spectrum usually is "bell-shaped" without any pronounced structure. Besides, a phenomenon called autofluorescence photobleaching (AFPB) normally takes place: its skin-emitted intensity decreases during continuous excitation and does not fully recover after interruptions of the excitation (Fig. 5).

## 3. AUTOFLUORESCENCE PHOTOBLEACHING: A TOOL FOR DISTANT SKIN ASSESSMENT

Several authors [8–10] observed that the skin autofluorescence intensity decreases with time during the laser exposure caused photobleaching according to the empirical double-exponential expression:

$$I(t) = a \exp(-t/\tau_1) + b \exp(-t/\tau_2) + A\,, \qquad (1)$$

where $a$ and $b$ are the weighting coefficients,
$A$ is a "bottomline" constant, and
$\tau_1$, $\tau_2$ are the fast and slow AFPB rates, respectively.

The "fast" AFPB (when sharp intensity decrease is observed) usually takes place during the first 5–15 seconds of irradiation, while the "slow" AFPB lasts up to several minutes.

Our initial studies [11, 12] have shown that the AFPB rates recorded from pigmented and vascular skin pathologies may essentially differ if compared with those recorded from the surrounding healthy skin. To investigate the clinical potential of photobleaching, a technology of imaging the skin AFPB rates was developed [13, 14]. The imaging setup (Fig. 6*A*) comprised an excitation laser coupled with an optical fibre for radiation delivery, a consumer camera equipped with a band-pass filter in front of the objective and operating at a slow video-mode (2 frames/s), and a computer with image processing software. As a result, parametric images of the $\tau$-value distribution over the imaged skin area have been obtained and analysed. In the regions of pigmented lesions (e.g. birthmarks or *nevi*) the $\tau_1$ values always exceeded those of the healthy skin – see Fig. 6*B*.

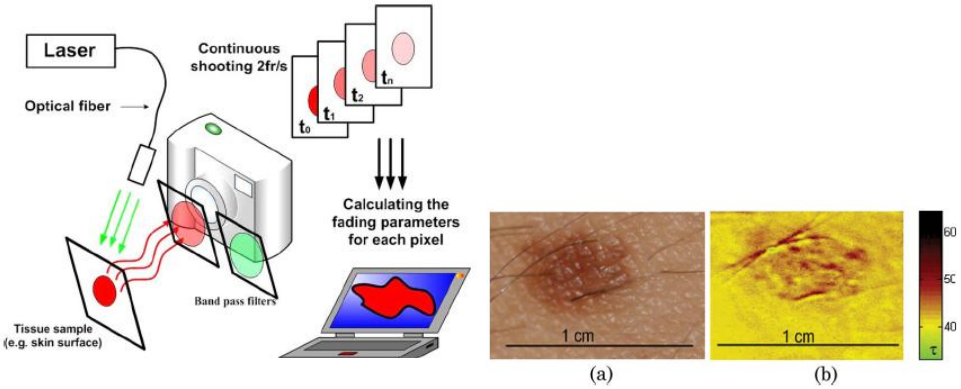


A B

*Fig. 6.* Experimental setup for imaging of skin AFPB rates (*A*), and comparison of a colour photo and parametric AFPB rate image of a pigmented skin nevus at 532 nm laser excitation (*B*) [13]. Colour scale: $\tau_1$ values in seconds multiplied by 10.

The developed imaging technique allowed experimental observation of the skin "photo-memory" effect: a weak visible laser irradiation at power density well below the standard skin safety limit (~200 mW/cm$^2$) leaves traces in the skin for several days [15]. These "fingerprints" (indicative of photo-induced structural changes of skin) can be detected by spectral imaging of autofluorescence as illustrated in Fig. 7 – skin was irradiated via a cross-shaped mask, and a day later the irradiated cross exhibited considerably lower autofluorescence intensity than the surrounding – previously non-irradiated – regions. Such observations lead to the conclusion that the existing laser skin safety standards have to be revised in order to avoid low-power laser (including laser pointer) caused skin damages.

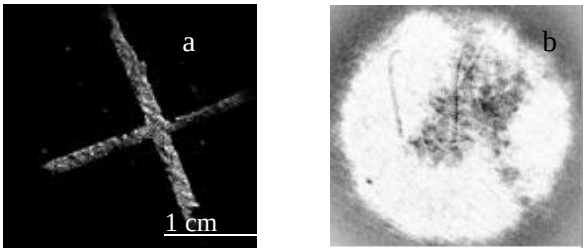


*Fig. 7.* Spectrally filtered AF images of normal skin under 405 nm laser irradiation (35 mW/cm$^2$): *a* – fluorescence image via the permeable cross mask, *b* – fluorescence image of the same skin area without mask, 24 h after irradiation [15].

The mechanism of skin AFPB has not been established in details so far. However, experimental evidence was obtained on a certain role of the skin chromophore melanin and oxy-haemoglobin in this process. The melanin-pigmented skin lesions exhibited slower AFPB than healthy skin, and increased melanin content in *nevi* correlated with a $\tau_1$ value decrease [9, 13]. The examinations of AFPB at the laser excitation wavelengths 405 nm and 532 nm (involving persons of all six skin photo-types) also showed the tendency to its slowing down with increased melanin content in epidermis (Fig. 8*a*). Increased oxy-haemoglobin content resulting from the low-power laser irradiation of healthy skin was observed both at fluorescence [10] and diffuse reflectance [16] spectra (Fig. 8*b*).

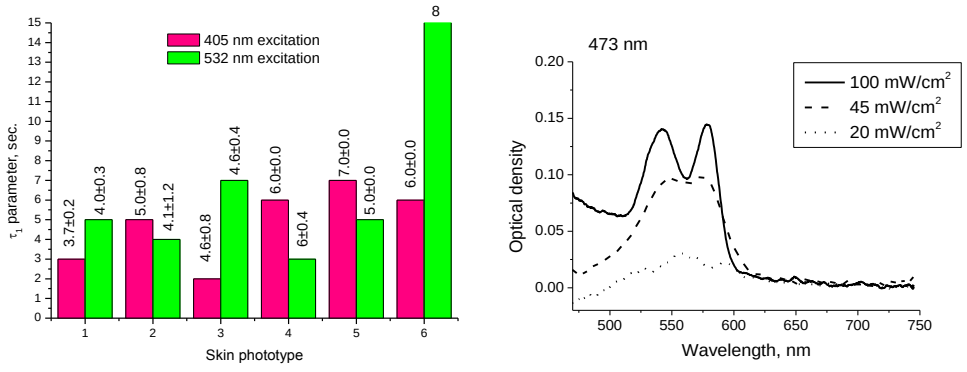


a b

*Fig. 8.* Correlation between the melanin content in skin epidermis and $\tau_1$ -values at laser (~ 70 mW/cm$^2$) wavelengths 405 nm and 532 nm [9] (*a*); appearance of oxy-haemoglobin absorption peaks in the post-irradiation diffuse reflectance spectra of skin [16] (*b*).

The latter may be indicative of some skin photo-inflammation (erythema), while the melanin role is still under discussions. Photo-induced production of epidermal melanin (like during the solar tanning of skin) that increases the light absorption thus decreasing the efficiency of skin fluorophore excitation seems to be a reasonable explanation. However, some multi-step photochemical reactions releasing active substances that destroy the surrounding fluorophores cannot be excluded as well. Presumably, the double-exponential character of photobleaching may point to a direct photo-damage of some fluorophores during the "fast" AFPB stage, with further slowing down due to backing off this process by the increased oxy-haemoglobin and melanin concentration in the irradiated skin.

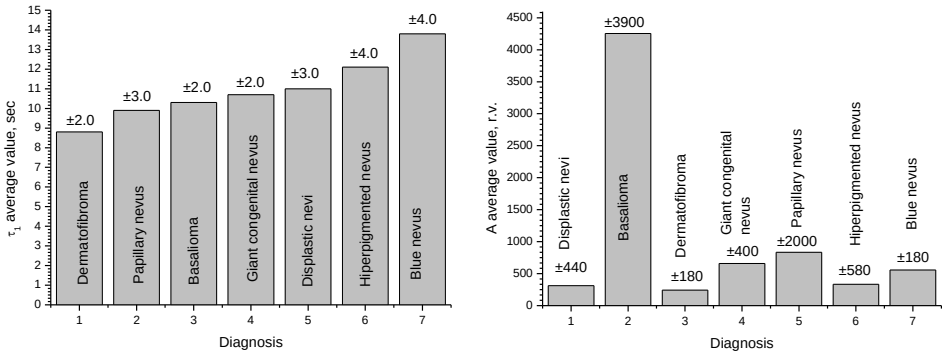


*Fig. 9.* Averaged values of autofluorescence photobleaching parameters $\tau_1$ (left) and *A* (right) for seven skin pathologies (532 nm laser excitation, power density ~ 65 mW/cm$^2$**)** [17].

In spite of uncertainty regarding the AFPB mechanism, the potential of AFPB rates and the bottom-line *A* value for quantitative diagnostics of various skin malformations have been clinically studied [17]. The obtained results confirm statistically significant differences of the $\tau_1$- and *A*-values (Fig. 9) for the selected seven skin lesions. The pronounced difference of *A*-values for skin basaliomas (Fig. 9, right) seems to be the most promising for further clinical implementation.

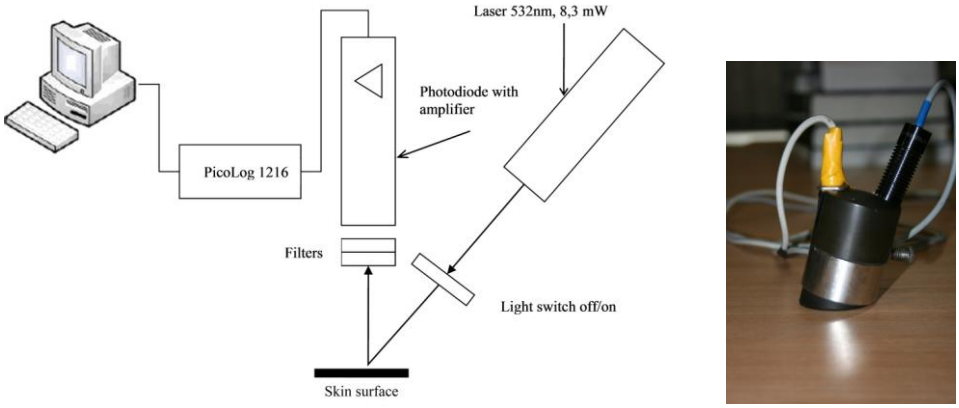


a b

*Fig. 10*. Design scheme (*a)* and view (*b*) of the prototype device for skin autofluorescence photobleaching measurements.

Figure 10 shows a compact prototype device designed for skin AFPB measurements at 532 nm laser excitation [18]. The device has been clinically tested. The whole fluorescence band is detected by means of a silicon photodiode and a set of band-pass filters in front of it; the output signals are processed by PC.

## 4. MULTISPECTRAL IMAGING: A TOOL FOR DISTANT MAPPING OF SKIN CHROMOPHORES

Another promising optical technology for distant *in-vivo* skin assessment is multispectral imaging (MSI). The principle of its operation is illustrated in Fig. 11.

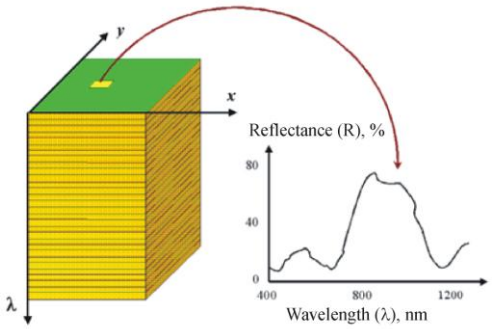


*Fig. 11*. Principle of multispectral imaging: acquisition and processing of the spectral image cube.

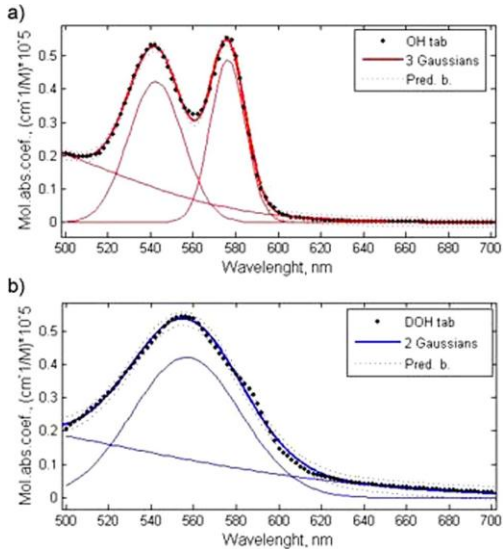


*Fig. 12.* Analytical approximation of oxy-haemoglobin and deoxy-haemoglobin absorption spectra by superposition of Gaussians within the spectral range 500–700 nm [19].

The basic idea is to take a set of spectral images of the same skin area, each at the neighbouring spectral band. After processing the image cube, reflectance spectra for each image pixel (i.e. for each "point" of the skin) can be restored. Specific spectral fitting algorithms can be further applied in order to create maps of parameters under interest, including the skin chromophore maps. It can be done

both numerically and analytically; the latter considerably saves time and computing resources. Analysis of the reference spectra allowed proposing handy analytic expressions that approximated well the tabular data within the spectral interval 500–700 nm. Superposition of three Gaussians proved to be optimal for approximation of the oxy-haemoglobin spectrum, while superposition of two Gaussians suited well for approximation of the deoxy-haemoglobin spectrum [19] – see Fig. 12. This opens the way to fit the measured skin reflectance spectra with those calculated in frame of the 3-chromophore model, assuming that the predicted optical density of the superficial skin layer can be expressed as

$$\mathrm{OD}(\lambda) = a_{\mathrm{OH}} \cdot \varepsilon_{\mathrm{OH}}(\lambda) + a_{\mathrm{DOH}} \cdot \varepsilon_{\mathrm{DOH}}(\lambda) + a_{\mathrm{Mel}} \cdot \varepsilon_{\mathrm{Mel}}(\lambda) + a_{Offset}, \qquad (2)$$

where $\varepsilon_{\mathrm{OH}}$, $\varepsilon_{\mathrm{DOH}}$ and $\varepsilon_{\mathrm{Mel}}$ correspond to the molar absorption spectra for oxy-haemoglobin (OH), deoxy-haemoglobin (DOH) and melanin (Mel);

$a_{OH}$, $a_{DOH}$ and $a_{Me}$ represent the relative chromophore concentration values;

$a_{Offset}$ is the difference between the predicted and the measured spectra.

Clinical measurements of various skin pathologies were taken by means of a high performance MSI camera *Nuance EX* with a tuneable liquid crystal filter (50 bands in the spectral range 450–950nm). A huge data set was collected, and clinically significant skin chromophore maps of the lesion areas were computed [20–24]; some examples are presented in Fig. 13. Spectral imaging appears helpful also for the recovery monitoring of vascular malformations after phototherapy [25].

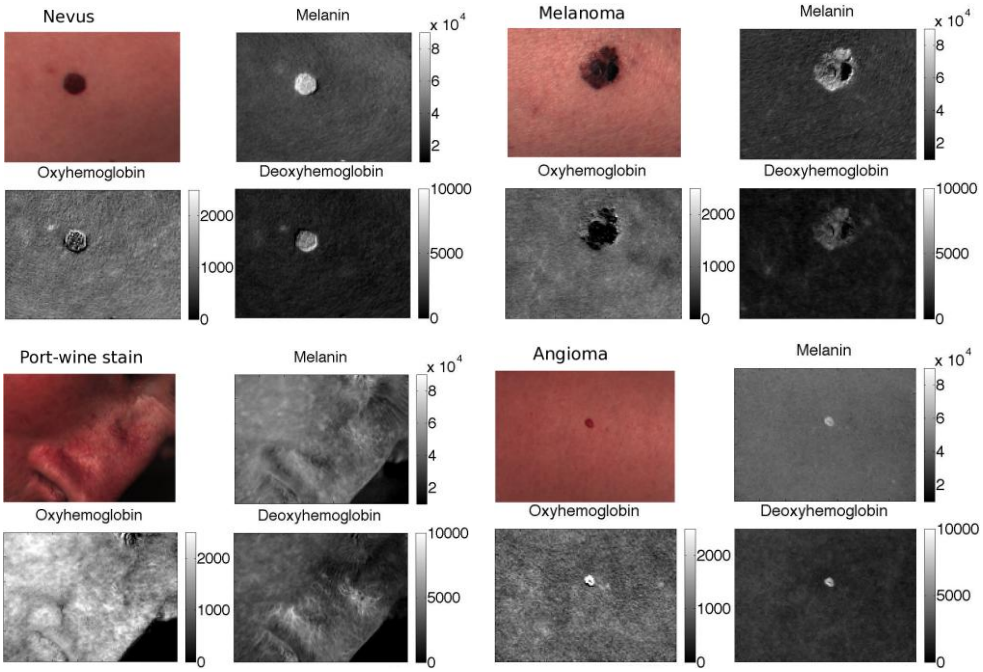


*Fig. 13.* RGB images of two pigmented and two vascular skin malformations with the corresponding skin melanin, oxy-haemoglobin and deoxy-haemoglobin maps [20].

Malignant melanoma (MM) is the deadliest skin cancer, so special attention is paid worldwide to its early diagnostics. Our skin MSI studies allow proposing two modalities of distant MM detection with relatively high sensitivity and specificity. One of them is based on correlation analysis of the melanin and haemoglobin content changes compared with the healthy skin [26, 27]. The correlation graphs allow extracting the MM regions separated from those of other skin pathologies (Fig. 14). The other proposed MM detection method is based on comparison of a limited number of skin spectral images. Analysis of clinical data made it possible to define an empirical parameter *p* depending on the optical densities at three selected spectral bands: ~540 nm, 650 nm and 950 nm; the parametric images of *p*-values can distinguish melanomas from other pigmented skin lesions like birthmarks [24, 28, 29] (Fig. 15). Advantage of this approach is a radically reduced number of the necessary spectral images – only three of them would be needed for the primary melanoma diagnostics.

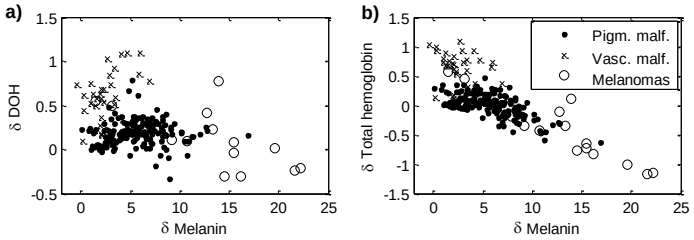


*Fig.14.* Correlation graphs of melanin and haemoglobin content changes (compared with the healthy skin) in melanomas, other pigmented malformations, and vascular lesions [26].

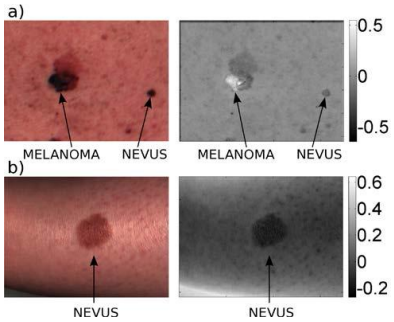


*Fig. 15.* Colour images (left) and parametric *p*-images (right) of melanoma and pigmented nevi [29]. $p = OD_{650} + OD_{950} - OD_{540}$ (*p*-value of healthy skin is set to 0).

Generally, also for mapping of the main skin chromophores and for some other skin-related parametric imaging there is no need to analyse a large number (50 or so) of spectral images. Proper processing may allow exploiting just 3…6 specifically selected spectral images; consequently, less complicated and more affordable equipment could be used for clinical diagnostics. Multispectral imaging by means of consumer-grade RGB digital cameras seems to be a promising option from this point, so series of studies on skin RGB imaging have been performed recently [30–37]. The main concept is to provide spectrally narrowband illumination of skin by colour LEDs or lasers for each selected spectral image, instead of sophisticated narrowband filtering in front of the image sensor at broadband white illumination.

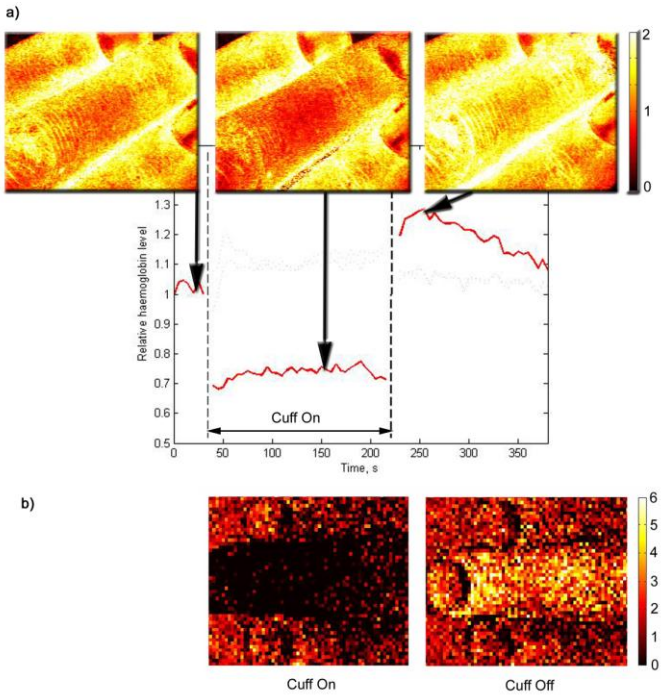


*Fig. 16.* Relative haemoglobin changes during middle finger cuff occlusion as reflected by RGB data at bi-chromatic laser illumination [34] (*a*) and by the conventional multispectral imaging at white illumination [19] (*b*).

The RGB single snapshot MSI at poly-chromatic skin illumination [34–37] is a novel low-budget technology that deserves a special attention. As an example, Fig. 16*a* illustrates the skin haemoglobin maps obtained from a single RGB image cube at bi-chromatic laser illumination (532 nm and 635 nm) [34]; these agree well with similar maps calculated from tens of spectral images taken by a commercial MSI camera *Nuance MX* (Fig. 16*b*). If linearity of the RGB sensor photo-response is ensured, simple logic allows extracting six spectral images from a single RGB image data set [34] or even more spectral images using a patented method [36].

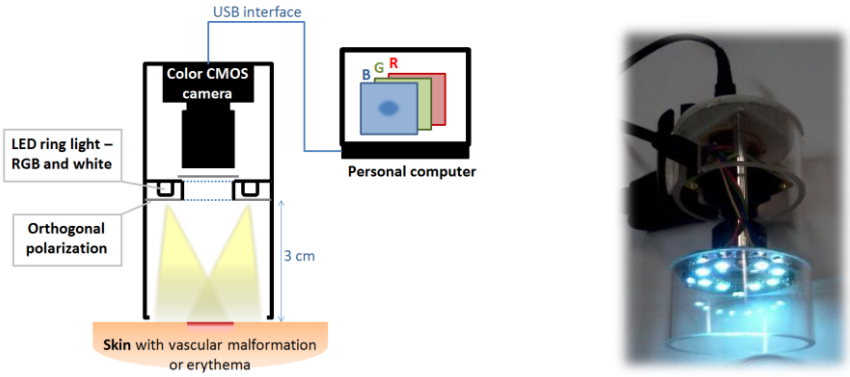


*Fig.17.* Design scheme and view of a prototype device for RGB mapping of skin chromophores [32].

A method and a device for reflectance RGB imaging simultaneously at several spectral bands have been patented recently [37]. A simple low-cost RGB camera and white LED based prototype device adapted for skin RGB imaging (Fig. 17) was designed and successfully tested in a number of clinical measurements [30–33].

## 5. MULTISPECTRAL PHOTOPLETHYSMOGRAPHY: A TOOL FOR SKIN MICROCIRCULATION ASSESSMENT

A novel photoplethysmography modality – multispectral PPG – has been developed in order to study skin blood pulsations at different vascular depths. The concept is based on the illustrated in Fig. 3*b* dependence of the mean penetration depth of light on its wavelength. In our early studies [38–40] the parallel detection of PPG signals at several wavelengths was provided by exploiting a CCD-based spectrometer also as the timer with temporal resolution ~50 ms, corresponding to the sampling rate of spectra ~20 $s^{-1}$. As a result, a 3-dimensional data cube was collected during the skin diffuse reflectance measurements, and processing of its cross-sections at fixed wavelengths revealed the AC signals or PPG pulsations at these wavelengths (Fig. 18*a*). The idea was experimentally implemented using two sets of three lasers with different wavelengths (405–532–645 nm and 645–807-1064nm) coupled with an optical fibre for simultaneous 3-wavelength skin irradiation at a single contact point (Fig. 18*b*).

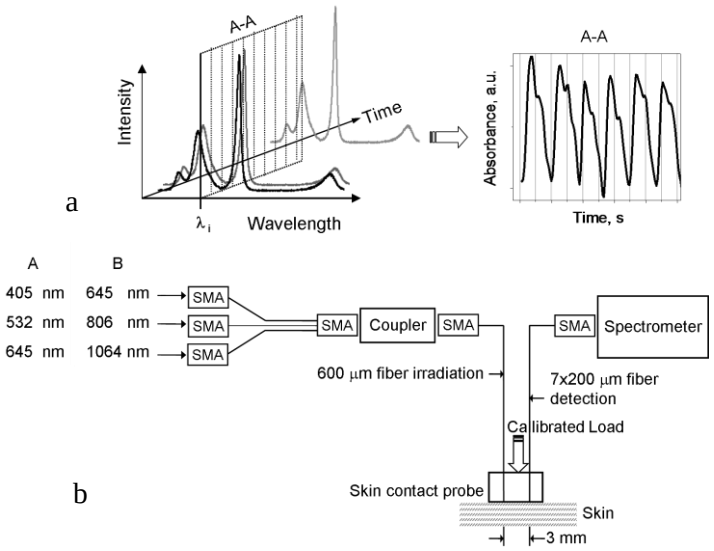


*Fig. 18.* Time-resolved PPG signal extraction from the intensity-wavelength-time data set (*a*); schematic of the multispectral PPG measurement setup (*b*) [38].

Clinical significance of the MS-PPG technique was demonstrated by the fingertip contact probe at simultaneous recordings of the spectral channel responses to external pressure and breath holding exercise. In both cases the responses at 405 nm and 532 nm illumination (shallow penetration) are very similar, including the absence of pulsations at the highest pressure applied (Fig. 19*a*) which points to full occlusion of the upper skin capillaries. The response at 645 nm (deeper

penetration) is different – no signs of occlusion at the highest applied pressure can be observed. Similarly, the red PPG signal baseline tends to increase during the breath holding, while the violet and green PPG baselines tend to decrease (Fig. 19*b*). The different MS-PPG responses obviously have physiological reasons and potentially might be used for non-invasive diagnostics in dermatology, surgery and cardiology.

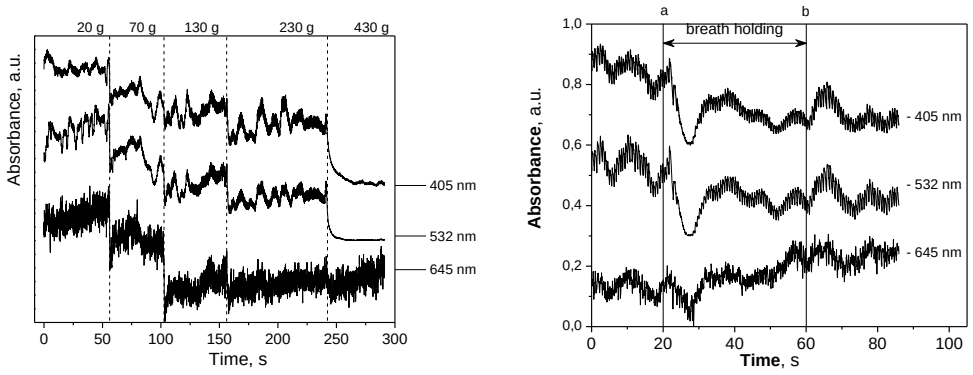


*Fig. 19*. Responses of multispectral PPG signals to increased external pressure (*a*) and breath holding (*b*) [39, 40].

Two other devices for multispectral PPG studies have been designed (Fig. 20) – one of them based on three-wavelength laser diode and the other – on the RGB LED and NIR LED [41–44]. Both devices have passed the first laboratory tests and currently are used in a series of clinical measurements.

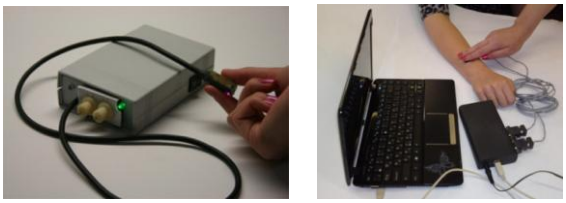

*Fig. 20*. Laser-based (*a*) and LED-based (*b*) prototype devices for multispectral PPG measurements [42, 43].

Nowadays, a clinical demand exists for non-invasive measurements of skin capillary refill time, e.g. to diagnose infant sepsis in an early stage. Blue light (400…450 nm) can penetrate only to the upper skin capillaries (Figs. 1*b*, 3*b*) and, therefore, blue remission is well suited for monitoring the capillary occlusion and refill. This was confirmed by experimental PPG-based capillary refill time measurements using a device comprising blue LED (420 nm) and infrared LED (940 nm) as light sources [45, 46] (Fig. 21*a*). Figure 21*b* shows how the blue PPG signals reflect capillary occlusion and refill; the NIR signal is used for pressure calibration – it reflects pulsations of deeper blood vessels and should remain pulsating while the blue pulsations disappear. Recently, another (more compact) blue LED based device with a mini-display has been developed for capillary refill time measurements [47].

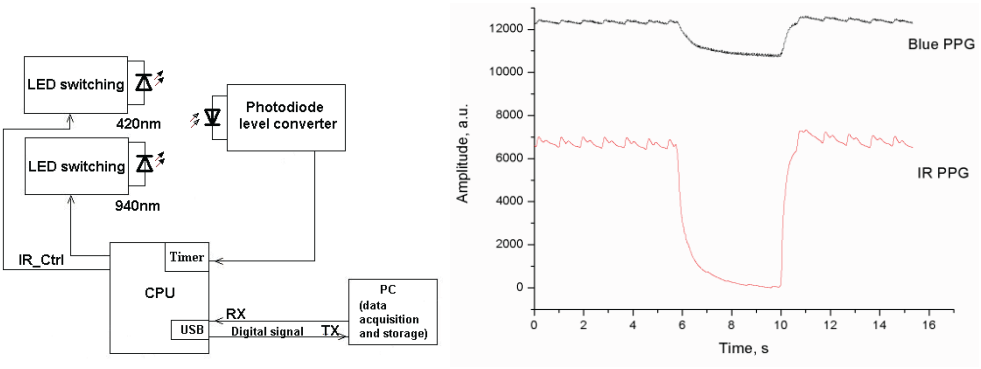


a b

*Fig. 21.* Block-diagram of the blue-NIR LED-based prototype device for capillary refill time measurement (*a*), and the 420 nm/940 nm remission PPG signal responses to external pressure (*b*) [46].

## 6. WIRELESS PHOTOPLETHYSMOGRAPHY: A TOOL FOR DISTANT MONITORING OF CARDIOVASCULAR CONDITION

Various designs of PPG sensor probes have been elaborated and tested, including those comprising wireless *Bluetooth* transmitters of the detected biosignals. Advantage of such devices is the possibility of long-term monitoring of the cardiovascular parameters (heartbeat rate and its variability, arterial elasticity, pulse wave transit time, PPG signal shape parameters, etc.) without movement limitations caused by the cable connections. Such sensors can be small, battery-powered and wearable, i.e. integrated in garments, goggles, earrings and other wearable items. At the present technology level, the battery resources may provide 10-h and longer continuous PPG monitoring at a distance to the signal receiver (e.g. computer, mobile phone) up to 20 m, so wearable PPG sensors may find applications for patient monitoring in hospitals and clinics, for self-monitoring at home, office and during physical exercises, for centralized sportsmen monitoring during trainings and competitions, etc.

*Fig. 22.* The wireless PPG finger probe with *Bluetooth* transmitter, and the "smart" hat with integrated forehead PPG sensor and transmitter [48, 49].

Apart from that, a wireless option of the conventional PPG finger clip (Fig. 22, left) has been developed [49] as well as some garments (hat, glove, sock, head-bandage, scarf, armband) with integrated miniature wireless PPG probes [48, 50]. A „smart" hat with a forehead probe is shown in Fig. 22 (right), and a set of simultaneously operating wireless PPG sensors integrated in head bandage, wrist strap, glove and scarf – in Fig. 23 (left). In this latter figure on the right the graph of correlation is shown between the heartbeat rate data measured by the wireless wrist strap sensor and those measured in parallel by a commercial ECG device – the reference for calibration.

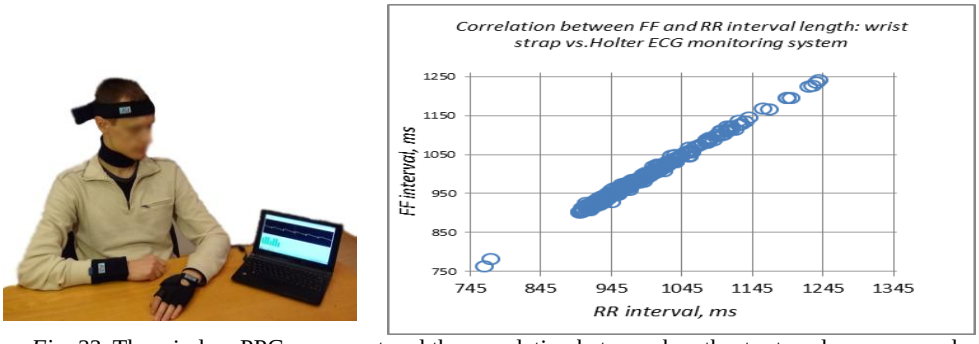


*Fig. 23.* The wireless PPG sensor set and the correlation between heartbeat rate values measured by the wrist strap sensor and Holter ECG device [50].

## 7. PHOTOPLETHYSMOGRAPHY VIDEO-IMAGING: A TOOL FOR DISTANT MAPPING OF SKIN BLOOD PERFUSION

The pulsatile remission PPG signals can be detected not only by specially designed skin contact probes, but also distantly by the video-imaging of skin. Any skin-reflected light, especially within the yellow-green range (where haemoglobin absorption is high and light can penetrate sufficiently deep into dermis), is slightly modulated with the heartbeat frequency due to periodic changes of the skin blood volume and the associated changes of the incident light absorption by blood haemoglobin.

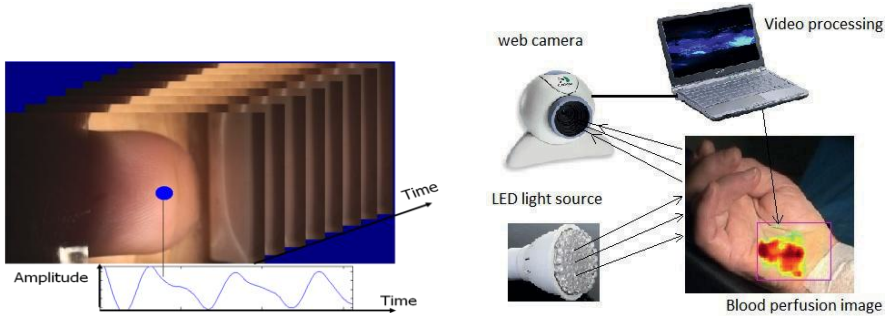


*Fig. 24.* Illustration of the PPG-imaging principle and the main components of a PPGI system [51].

Figure 24 illustrates the principle of PPG-imaging. The video-signal consists of a number of image frames taken at a definite frame rate, e.g. 20 frames per second. Consequently, during one heart activity cycle (~1 s) 20 skin images are obtained, each at different phase of the pulse wave that travels via the skin blood vessels. If consecutive frames are compared, the reflected light intensity detected at the same image area increases/decreases with time, forming a periodic PPG signal. Specific software [51, 52] allows extracting the PPG pulsations from the video-signal over the whole skin image area. The amplitude of PPG peaks may differ between the image pixels due to different blood supply or perfusion of the skin tissues (especially if there is a burn or other skin damage). After proper processing, the adequate parametric maps of the PPG signal amplitude distribution (or blood perfusion maps) can be constructed [52, 53]. The laboratory-made PPGI prototype device is presented in Fig. 25. It contains a stabilized white illumination source

comprising 80 LEDs and a CMOS RGB 752×480 pixel video-camera with objective lens; both are mounted on the same holder. This device was successfully applied for distant anaesthesiology control during arm surgery; good correlation between the PPG signal amplitude and the skin temperature was obtained, i.e. the skin perfusion jump signalling about the action of anaesthetics was detected remotely (Fig. 26*a*) [53].

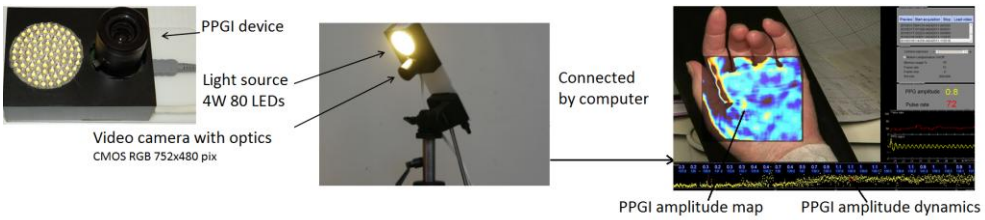


*Fig. 25.* Schematic of the developed PPGI prototype device [53].

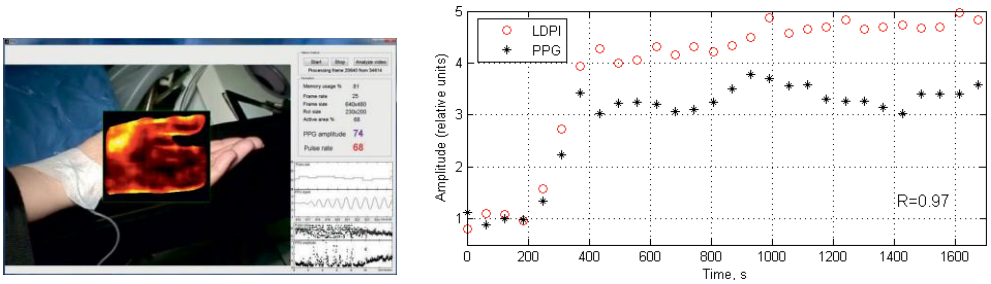


a b

*Fig. 26.* Clinical measurements of skin blood perfusion during anaesthesia (*a*); the PPGI signal correlation with blood perfusion as measured by LDF (*b*) [52, 53].

The technology was recently patented [54] and may become routine for remote control of anaesthesia during surgeries. Similarly, good correlation with the recordings of commercial laser-Doppler flowmeter (LDF) was obtained when blood perfusion changes during the skin heat test (Fig. 26*b*) were detected [52, 53]. So, the skin blood perfusion mapping by PPGI technology seems to be competitive with the routinely used LDF technique.

These two examples confirm the clinical potential of PPGI devices and strongly motivate to develop them further, aiming at real implementation in the everyday clinical practice.

## 8. CONCLUSIONS

The above presented results confirm good future prospects of the developed biophotonic technologies for a wide range of clinical applications in dermatology, surgery, cardiology, and related specialties. Their main advantages are patient-friendly non-invasiveness, compactness, fast (even real-time) response, relatively simple design, ease of use, and low cost. The reported proofs of concepts may be further developed in collaboration with the healthcare professionals and medical equipment manufacturers in order to produce advanced diagnostic and monitoring devices for the everyday use in hospitals, clinics and personalised healthcare.

*ACKNOWLEDGEMENTS*

*This study was funded from several sources, including the European Social Fund project #2009/0211/1DP/1.1.1.2.0/09/APIA/VIAA/077 "Biophotonics research group" and the European Regional Development Fund project #2010/0271/2DP2/2.1.1.1.0/APIA/VIAA/030 "Novel optical technologies for complex non-contact diagnostics of skin". Author is truly grateful to all laboratory personnel, first of all to his past and present PhD students R. Erts, U. Rubins, A. Lihachev, I. Kuzmina, D. Jakovels, E. Kviesis-Kipge, I. Diebele, and others. The clinical support by medical doctors I. Kukulis, K. Rozniece, L. Valeine, A. Berzina, A. Deryabo, J. Kapostinsh, A. Miscuks and others is highly appreciated.*

REFERENCES

1. A European strategy for Key Enabling Technologies – a bridge to growth and jobs: http://ec.europa.eu/enterprise/sectors/ict/key_technologies/index_en.htm.
2. http://www.medterms.com/script/main/art.asp?articlekey=3278.
3. Ugnell, H., & Öberg, P.Å. (1995). Time variable photoplethysmography signal: its dependence on light wavelength and sample volume. *Proc. SPIE*, 2331, 89–97.
4. Allen, J. (2007). Photoplethysmography and its application in clinical physiological measurement. *Physiol. Meas., 28,* R1-R39.
5. Boulnois, J. (1986). Photophysical processes in recent medical laser developments, *Las. Med. Sci*., (1), 47–66.
6. Anderson, R., & Parrish, J. (1981). The optics of human skin. *J. Invest. Derm*., *77*, 13–18.
7. Wagnieres, G., Star, W., & Wilson, B. (1998). In vivo fluorescence spectroscopy and imaging for oncological applications. *Photochem. Photobiol*., *68*(5), 603–632.
8. Stratonnikov, A.A., Polikarpov, V.S., & Loschenov, V.B. (2001). Photobleaching of endogenous fluorochroms in tissues *in vivo* during laser irradiation. *Proc. SPIE, 4241*, 13–24.
9. Lihachev, A. (2011). *Kinetics of laser excited in-vivo skin autofluorescence and remission*. PhD Thesis, Riga: University of Latvia.
10. Lesinsh, J., Lihachev, A., Rudys, R., Bagdonas, S., & Spigulis, J. (2011). Skin autofluorescence photobleaching and photo-memory. *Proc. SPIE*, 8092, 80920N.
11. Lihachev, A., & Spigulis, J. (2007). Skin autofluorescence fading at 405/532 nm laser excitation. *IEEE Xplore*, 10.1109/NO, 63-65.
12. Spigulis, J., Lihachev, A., Gailite, L., & Erts, R. (2008). Novel laser technologies for human skin *in-vivo* assessment. *Proc. SPIE*, 7022**,** 70220N.
13. Spigulis, J., Lihachev, A., & Erts, R. (2009). Imaging of laser-excited tissue auto-fluorescence bleaching rates. *Appl. Opt., 48*(10), D163-D168.
14. Jakovels, D., & Spigulis, J. (2010). RGB imaging of laser-excited skin autofluorescence bleaching rates. *Proc. SPIE*, 7376, 737618.
15. Lihachev, A., Lesins, J., Jakovels, D., & Spigulis, J. (2010). Low power CW-laser signatures on human skin. *Quant.Electron., 40*(12), 1077–1080.
16. Ferulova I., Lesins, J., Lihachev, A., Jakovels, D., & Spigulis, J. (2012). Influence of low power CW laser irradiation on skin hemoglobin changes. *Proc. SPIE*, 8427, 84273I.
17. Lihachev, A., Rozniece, K., Lesins, J., & Spigulis, J. (2011). Photobleaching measurements of pigmented and vascular skin lesions: results of a clinical trial. *Proc. SPIE*, 8087, 80872F.
18. Ferulova, I., Rieba, A., Lesins, J., Berzina, A., Lihachev, A., & Spigulis, J. (2012). Portable device for skin autofluorescence photobleaching measurements. *Lith. J. Phys*., *52*(1), 55–58.

19. Jakovels, D., & Spigulis, J. (2010). 2-D mapping of skin chromophores in the spectral range 500-700 nm. *J. Biophoton.*, *3*(3), 125–129.
20. Kuzmina, I., Diebele, I., Valeine, L., Jakovels, D., Kempele, A., Kapostinsh, J., & Spigulis, J. (2011). Multi-spectral imaging analysis of pigmented and vascular skin lesions: results of a clinical trial. *Proc. SPIE*, 7883, 788312.
21. Jakovels, D., Spigulis J., & Saknite, I. (2010). Multi-spectral mapping of in-vivo skin haemoglobin and melanin. *Proc. SPIE*, 7715, 77152Z1-4.
22. Kuzmina, I., Asare, L., Diebele, I., Jakovels, D., Kempele, A. & Spigulis, J. (2010). Multispectral imaging of pigmented and vascular cutaneous malformations: the influence of laser treatment. *Proc. SPIE*, 7376, 73760J.
23. Saknite, I., Jakovels, D. & Spigulis, J. (2011). Distant determination of bilirubin distribution in skin by multi-spectral imaging. *Latv.J.Phys.Tech.Sci.*, *48* (2), 50-55.
24. Diebele, I., Bekina, A., Derjabo, A., Kapostinsh, J., Kuzmina, I. & Spigulis, J. (2012). Analysis of skin basalioma and melanoma by multispectral imaging. *Proc. SPIE* 8427, 842732.
25. Kuzmina, I., Diebele, I., Spigulis, J., Valeine, L., Kempele, A. & Abelite, A. (2011). Contact and contactless diffuse reflectance spectroscopy: potential for recovery monitoring of vascular lesions after intense pulsed light treatment. *J. Biomed. Opt.*, *16* (4), 040505.
26. Kuzmina, I., Diebele, I., Jakovels, D., Spigulis, J., Valeine, L. & Kapostinsh, J. (2011). Towards noncontact skin melanoma selection by multispectral imaging analysis, *J. Biomed. Opt.*, *16* (6), 060502.
27. Kuzmina, I. (2011). *Contact and contactless diffuse reflectance spectrometry for assessment of skin pathologies*. PhD Thesis, Riga: University of Latvia.
28. Diebele, I., Kuzmina, I., Kapostinsh, J., Derjabo, A. & Spigulis, J. (2011). Melanoma-nevus differentiation by multispectral imaging. *Proc. SPIE*, 8087, 80872G.
29. Diebele, I., Kuzmina, I., Lihachev, A., Spigulis, J., Kapostinsh, J., Derjabo, A. & Valeine, L. (2012). Clinical evaluation of melanomas and common nevi by spectral imaging. *Biomed.Opt.Express, 3* (3), 467–472.
30. Jakovels, D., Spigulis, J. & Rogule, L. (2011). RGB mapping of hemoglobin distribution in skin. *Proc. SPIE*, 8087, 80872B.
31. Jakovels, D., Spigulis, J. (2011). RGB imaging system for mapping and monitoring of hemoglobin distribution in skin. *Proc. SPIE*, 8158, 8158OR.
32. Jakovels, D., Spigulis, J. (2012). RGB imaging device for mapping and monitoring of hemoglobin distribution in skin. *Lith. J.Phys.*, *52* (1), 50–54.
33. Jakovels, D., Kuzmina, I., Berzina, A. & Spigulis, J. (2012). RGB imaging system for monitoring of skin vascular malformation's laser therapy. *Proc. SPIE* 8427, 842737.
34. Spigulis, J., Jakovels, D. & Rubins, U. (2010). Multi-spectral skin imaging by a consumer photo-camera. *Proc. SPIE* 7557, 75570M.
35. Spigulis, J., Jakovels, D. & Elste, L. (2012). Towards single snapshot multispectral skin assessment. *Proc. SPIE* 8216, 82160L.
36. Spigulis, J., Jakovels, D. & Rubins, U. (2012). Method and device for multi-spectral imaging by means of a digital RGB sensor. Patent WO 2012/002787 A1; (2010) Latvian patent LV 14207 B.
37. Spigulis, J., & Elste, L. (2012). Method and device for imaging of spectral reflectance at several spectral bands, Latvian patent LV 14532 B.
38. Spigulis, J., Gailite, L., Lihachev, A. & Erts, R. (2007). Simultaneous recording of skin blood pulsations at different vascular depths by multi-wavelength photoplethysmo-graphy. *Appl. Opt. 46* (10), 1754–1759.
39. Gailite, L., Spigulis, J., & Lihachev, A. (2008). Multilaser photoplethysmography technique. *Las. Med. Sci.*, *23* (2), 189–193.
40. Spigulis, J., Gailite, L. & Lihachev, A. (2007). Contact probe pressure effects in skin multi-wavelength photoplethysmography. *Proc. SPIE-OSA*, 6628, 66281F.

41. Asare, L., Kviesis–Kipge, E., Grabovskis, A., Rubins, U., Erts, R. & Spigulis, J. (2011). Multi-spectral photoplethysmography biosensor. *Proc. SPIE*, 8073, 80731Z.
42. Asare, L., Kviesis-Kipge, E., Rubins, U., Rubenis, O. & Spigulis, J. (2011). Multi-spectral photoplethysmography technique for parallel monitoring of pulse shapes at different tissue depths. *Proc. SPIE*, 8087, 80872E.
43. Asare, L., Kviesis-Kipge, E., Ozols, M., Spigulis, J. & Erts, R. (2012). Multi-spectral optoelectronic device for skin microcirculation analysis. *Lith. J.Phys*., *52*(1), 59-62.
44. Asare, L., Ozols, M., Rubins, U., Rubenis, O. & Spigulis, J. (2012). Clinical measurements with multi-spectral photoplethysmography sensors. *Proc. SPIE* 8427, 842734.
45. Kviesis-Kipge, E., Curkste, E., Spigulis, J. & Gardovska, D. (2009). Optical studies of the capillary refill kinetics in fingertips. *Proc. IFMBE 25/VII*, 377-379.
46. Kviesis-Kipge, E., Curkste, E., Spigulis, J. & Eihvalde, L. (2010).Real-time analysis of skin capillary-refill processes using blue LED. *Proc. SPIE*, 7715, 7715231-5.
47. Laksa, E., Zaharans, J. & Rubenis, O. (2012). Device for measurement of capillary blood refill time. Abstr. Int. Conf. *"Biophotonics in Dermatology and Cardiology"*, Riga, p.34.
48. Spigulis, J., Erts, R., Nikiforovs, V. & Kviesis-Kipge, E. (2008). Wearable wireless photoplethysmography sensors. *Proc. SPIE* 6991, 6991120.
49. Erts, R., Kviesis-Kipge, E., Zaharans, J., Zaharans, E. & Spigulis, J. (2010). Wireless photoplethysmography finger sensor probe, *IEEE Explore*, 10.1109/BEC.2010.5630194, 283–284.
50. Kviesis-Kipge, E., Mecnika, V. & Rubenis, O. (2012). Miniature wireless photoplethysmography devices: integration in garments and test measurements. *Proc. SPIE* 8427, 84273H.
51. Erts, R., Rubins, U. & Spigulis, J. (2009). Monitoring of blood pulsation using non-contact technique, *Proc. IFMBE* 25/VII, 754–756.
52. Rubins, U., Erts, R. & Spigulis, J. (2010). The blood perfusion mapping in the human skin by photoplethysmography imaging, *Proc. IFMBI*, *29*, 304–306.
53. Rubins, U., Upmalis, V., Rubenis, O., Jakovels, D. & Spigulis, J. (2011). Real-time photoplethysmography imaging system. *Proc. IFMBE, 34*, 183–186.
54. Miscuks, A., Erts, R., Rubins, U., Spigulis, J., & Mihelsons, M. (2012). Method and device for determination of regional anaesthesia by means of contactless photoplethysmography. Latvian patent LV14444.

## BIOFOTONIKAS TEHNOLOĢIJAS NEINVAZĪVAM ĀDAS STĀVOKĻA UN ASINS MIKROCIRKULĀCIJAS NOVĒRTĒJUMAM

J. Spīgulis

Kopsavilkums

Sniegts pārskats par autora laboratorijā pēdējo piecu gadu laikā iegūtajiem *in-vivo* ādas optiskā novērtējuma svarīgākajiem rezultātiem. Īsumā aplūkotas dzīvas ādas optiskās īpašības, turpinājumā aprakstot jaunradītās metodes un prototipa ierīces. Piedāvātas, eksperimentāli realizētas un klīniski pārbaudītas sešas neinvazīvas diagnostikas un monitoringa tehnoloģijas, kas balstītas uz ādas autofluorescences fotoizbalēšanu, difūzās refleksijas spektrometriju, multispektrālu ādas attēlošanu un remisijas fotopletizmogrāfiju.

03.06.2012.